Tuning anion solvation energetics enhances potassium–oxygen battery performance

Shrihari Sankarasubramanian[a,b], Joshua Kahky[b], and Vijay Ramani[a,b,1]

[a]Center for Solar Energy and Energy Storage, Washington University in St. Louis, St. Louis, MO 63130; and [b]Department of Energy, Environmental & Chemical Engineering, Washington University in St. Louis, St. Louis, MO 63130

Edited by Alexis T. Bell, University of California, Berkeley, CA, and approved June 21, 2019 (received for review January 23, 2019)

The oxygen reduction reaction (ORR) is a critical reaction in secondary batteries based on alkali metal chemistries. The nonaqueous electrolyte mediates ion and oxygen transport and determines the heterogeneous charge transfer rates by controlling the nature and degree of solvation. This study shows that the solvent reorganization energy (λ) correlates well with the oxygen diffusion coefficient (D_{O_2}) and with the ORR rate constant (k) in nonaqueous Li–, Na–, and K–O_2 cells, thereby elucidating the impact of variations in the solvation shell on the ORR. Increasing cation size (from Li^+ to K^+) doubled k/λ, indicating an increased sensitivity of k to the choice of anion, while variations in D_{O_2} were minimal over this cation size range. At the level of a symmetric K–O_2 cell, both the formation of solvent-separated ion pairs [K^+–$(DMSO)_n$–ClO_4^- + $(DMSO)_m$–ClO_4^-] and the anions being unsolvated (in case of PF_6^-) lowered ORR activation barriers with a 200-mV lower overpotential for the PF_6^- and ClO_4^- electrolytes compared with OTf^- and $TFSI^-$ electrolytes with partial anion solvation [predominantly K^+–$(DMSO)_n$–OTf^-]. Balancing transport and kinetic requirements, KPF_6 in DMSO is identified as a promising electrolyte for K–O_2 batteries.

metal–oxygen battery | oxygen reduction reaction | electrochemical kinetics | solvent reorganization energy

Nonaqueous, secondary alkali and alkaline earth metal–oxygen batteries promise some of the highest theoretical specific energies (*SI Appendix*, Fig. S1). Thus, the oxygen reduction reaction (ORR) is the key to the rapid growth of battery specific energy density required for long-range electric transportation, ever-more energy-intensive electronic devices, and long-duration (10 to 100 h per cycle) energy storage (1–3). Since the demonstration of the secondary Li–O_2 cell by Abraham and Jiang (4), the ORR in nonaqueous electrolytes has been the subject of sustained interest (5–7). Unfortunately, Li–O_2 batteries suffer due to the high-energy barrier to the oxygen evolution reaction (OER) (1, 8), parasitic side reactions (9), Li dendrite growth (10), and unstable electrolytes (11–14). Despite the development of OER catalysts (15–20), water stable and oxidatively stable (14, 21, 22) electrolytes for the Li–O_2 system, the Li_2O_2 discharge product (ΔG^0 = −570.8 kJ·mol^{-1}) (23) requires a large OER overpotential, drastically lowering energy efficiency (24). The Na–O_2 system suffers from similar problems (25–28), where the lower OER potentials and resultant decrease in electrolyte degradation is offset by the greater chemical reactivity of Na (29). Research into Mg–O_2 (30) [note the highly pyrophoric nature of Mg electrolytes (31, 32)] and Ca–O_2 cells (33) (ion transport limited by bulky Ca^+ cations) are still in their infancy.

The K–O_2 battery, first reported by Ren and Wu (34), offers a high theoretical specific energy value of 935 Wh·kg^{-1} in a low overpotential system. The 1-electron transfer ORR in this system results in potassium superoxide (KO_2) being the discharge product. The thermodynamic stability of KO_2 (ΔG^0 = −239.4 kJ·mol^{-1}) (34) mitigates the thermodynamic barriers inherent in 2-electron OER in Li–O_2 and Na–O_2 cells where the corresponding alkali metal peroxide is the dominant product. K–O_2 exhibit lower theoretical energy density and specific capacity compared with Li–O_2 cells [comparable to Li-S cells (9)], but their far greater reversibility offsets these losses.

The development of the K–O_2 system is in a nascent stage and the cell performance (35), dendrite mitigation at the metallic anode (36), possible side reactions (37), solid electrolyte interphase formation (38), the long-term stability of the discharge product (39), and routes to achieve practical charge and discharge currents have been examined (5, 40). These efforts are summarized in the recent review by Wu and coworkers (41).

This study extends the fundamental kinetic understanding of the ORR in a K–O_2 cell achieved in the work of Sankarasubramanian and Ramani (5) and examines the influence of the electrolyte formulation on the ORR in K–O_2 cells. The influence of the solvent on the solubility and the solvation of the salt has been previously studied in other alkali metal–oxygen cells in terms of both the Pearson hard–soft acid–base (HSAB) theory (42) and in terms of the solvent reorganization energy (λ) from Marcus–Hush theory (7). Furthermore, it has been shown that the ORR in Li–O_2 and Na–O_2 cells, which are analogous to K–O_2 cells, displays a strong dependence on the electrolyte solvent (42–47), salt (48, 49), and additives present (22, 50–53). The K^+ ion has a lower charge density (a softer acid compared with Li^+ in HSAB parlance) and hence may display a greater tendency to form solvated ion pair complexes. Dimethyl sulfoxide (DMSO)-based electrolytes lead to significantly faster first electron transfer kinetics in the ORR (5). This study examines the solvent reorganization energy required to initiate ORR in the presence of different counterions and demonstrates that partial solvation of the anion is detrimental to both ORR kinetics and overall cell performance. Thus, effective solvation with high donor number solvents (more significant for high charge density cations like Li^+) and judicious selection of salt anions (more significant for lower charge density cations like Na^+, K^+) results in solution stabilization (high λ) or

Significance

Potassium–oxygen (K–O_2) batteries are a high-energy alternative to Li-ion batteries. They produce KO_2 as the discharge product in a highly reversible reaction, circumventing the electrolyte stability and rechargeability challenges of other alkali metal–oxygen batteries. Herein, a pathway is presented for the multifold increase of the practical discharge power of these batteries by tailoring the tripartite interactions between the salt cation and anion and the solvent. A single descriptor of the solvation energetics captures the influence of electrolyte composition on reactant transport and reaction kinetics and is broadly applicable to alkali metal–oxygen (i.e. Li–, Na–, and K–O_2) batteries, providing a rational basis to design electrolyte compositions for high-power alkali metal–oxygen batteries.

Author contributions: S.S. conceived and initiated research; S.S. and V.R. designed research; S.S. and J.K. performed research; S.S. contributed new reagents/analytic tools; S.S. and V.R. analyzed data; and S.S. and V.R. wrote the paper.

The authors declare no conflict of interest.

This article is a PNAS Direct Submission.

[1]To whom correspondence may be addressed. Email: ramani@wustl.edu.

This article contains supporting information online at www.pnas.org/lookup/suppl/doi:10.1073/pnas.1901329116/-/DCSupplemental.

Published online July 10, 2019.

ENGINEERING

surface stabilization (low λ) of the O_2/O_2^- redox couple, significantly improving the ORR kinetics in alkali metal–oxygen batteries.

Results and Discussion

Fig. 1*A* depicts the 3-component interactions between the cation and anion of the salt and the solvent in an electrolyte solution. All further discussion is best understood in the context of Pearson's HSAB theory, which necessitates the introduction of the key concepts of the donor number (DN) and acceptor number (AN) [defined by Gutmann (54, 55)], which provide a somewhat quantitative measure of the Lewis basicity and acidity of a given chemical species, respectively. In the context of the ionic salts [with partial positive (δ^+) and partial negative (δ^-) charge centers], the solute anions possess the ability to donate electrons toward the cation. Depending on the solvent, the cation and anion together can be covered by a solvent shell to form contact ion pairs (poor solvation), the cation and anion can be completely solvated and separated from each other to form solvent-separated ion pairs (typical of highly polar solvents), or either the cation or anion may be preferentially solvated if the solvent has a high DN (and relatively low AN) or high AN (and relatively low DN), respectively (45, 55). Thus, while a nonpolar solvent like acetonitrile (MeCN) (with low DN and AN) dissolves alkali metals salts up to concentrations of 0.5 M (42), a solvent with a higher donor number like DMSO can dissolve alkali metal salts up to 1 M (5, 7).

The DMSO used in this study was chosen as it would be highly solvating (with the degree of cation and anion solvation to be examined), while the salts were selected to offer a range of anion solvation behaviors (structures, DN and AN values provided in Fig. 1 *B–F*) (5, 40, 55–59). DMSO has a higher DN than any of the anions and should easily solvate the K^+ ion, while the low AN of DMSO renders complete solvation of the anions unlikely.

Fig. 2 depicts the possible reaction pathways for the ORR in K–O_2 cells. The pathways shown in black are substantiated by experimental observations, while the gray pathways are proposed based on our best understanding. The formation of KO_2 as the discharge product in K–O_2 cells has been extensively documented (5, 34, 39, 40). There is some indication (5, 40) that KO_2 may react further, but K_2O_2 has not yet been detected in K–O_2 cells. The initial step in the ORR is the 1-electron reduction of dissolved O_2 to either the superoxide (O_2^-) ion or KO_2. Depending on the DN of the solvent and binding energy of reactant species on the

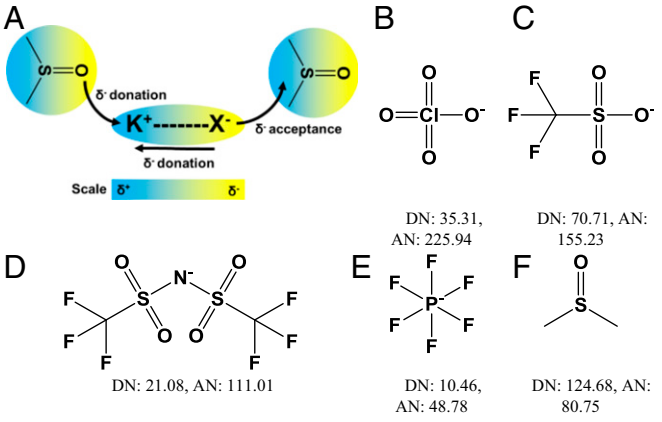

Fig. 1. (*A*) Schematic representation of the solvent–salt (KX where X is the anion) interactions in the electrolyte (the charge distributions are only illustrative and do not represent actual electron density or distribution) and chemical structures of the potassium salt anions investigated: (*B*) perchlorate, (*C*) trifluoromethanesulfonate, (*D*) bis(trifluoromethanesulfonyl)imide, (*E*) hexafluorophosphate, and the solvent (*F*) DMSO.

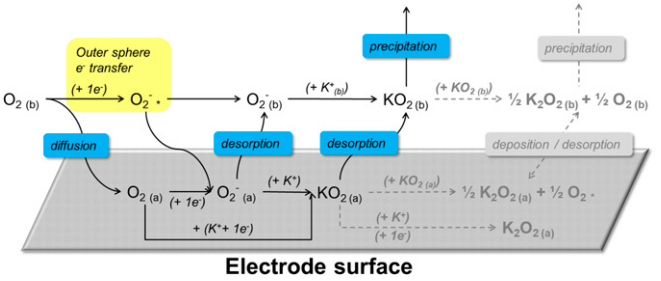

Fig. 2. ORR reaction scheme in a K–O_2 cell. The possible further reactions of KO_2 to form K_2O_2 (based on our current understanding) are depicted in gray.

electrode, this may occur by either an outer-sphere or inner-sphere process. The superoxide thus formed may either be stabilized in solution by coordinating with the solvated cation or by adsorbing onto the electrode surface. Electrolyte solvents with high DNs would tend to coordinate with a highly electrophilic species such as K^+, which is a relatively small ion with a high charge density (albeit lower than both Li^+ and Na^+) and hence is a hard Lewis acid. The coordination with a high DN solvent such as DMSO would increase the ionic radius without changing the overall charge on the complex, thus lowering the charge density and rendering the K^+–$(solvent)_n$ complex a soft Lewis acid. According to the HSAB theory, this soft Lewis acid can then coordinate with the soft Lewis base O_2^- and form a solvent-separated K^+–$(solvent)_n$–O_2^- ion pair with further reduction occurring via the solution-based route.

K^+ salts can be expected to form solvent-separated ion pairs in solution in DMSO where the cation is completely solvated and is paired with a unsolvated (or minimally solvated) anion. Thus, we expect a competition in solution between the formation of the K^+–$(DMSO)_n$–O_2^- and K^+–$(DMSO)_n$–X^- ion pairs. This would influence the proportion of O_2 reacting in solution vs. on the surface, the solubility of KO_2, the stability of KO_2 formed in solution, and the O_2 diffusion coefficient. The outcome of this competition will determine the reaction route followed by the ORR, with superoxide stabilization in solution resulting in a predominantly solution-based ORR and the lack of such stabilization leading to the surface reaction being dominant. The K^+ solvation sphere is a 3-body system with cation–anion, cation–solvent, and anion–solvent interactions and a single solvent property is not expected to capture the effects of all these interactions [as seen from the discussion regarding the DN, AN, and solvent reorganization energy in our previous work (7)]. Before addressing the effect of the electrolyte formulation on oxygen and the superoxide ion, the degree of cation and anion solvation and possible cation–anion interactions were spectroscopically examined.

Fourier transform infrared (FTIR) spectra recorded in DMSO electrolytes with $KClO_4$, KOTf, KPF_6, and KTFSI salts are shown in Fig. 3 *A–D*, respectively (the instrumentation is described in *SI Appendix*, and spectra over a larger frequency range is depicted in *SI Appendix*, Fig. S2). The spectra were recorded with 3 different salt concentrations (0.1, 0.5, and 1 M), and the spectra of pure DMSO and the salt are provided for comparison. The spectrum of DMSO displayed the characteristic symmetric stretching vibration of the S=O group at 1,050 cm^{-1} and a peak at 1,020 cm^{-1} corresponding to the rocking vibrations of the methyl groups (60). In case of all 3 salts, the relationship between the intensities of the characteristic salt counterion peaks in the electrolytes and the salt concentrations in solution indicates the degree of anion solvation. Furthermore, the association of the anions with the solvated cation has been found to result in the characteristic peaks of the anions, either splitting or changing frequencies (48, 61). A combination of these characteristics was used to deconvolute the solvation structures in the electrolytes under consideration.

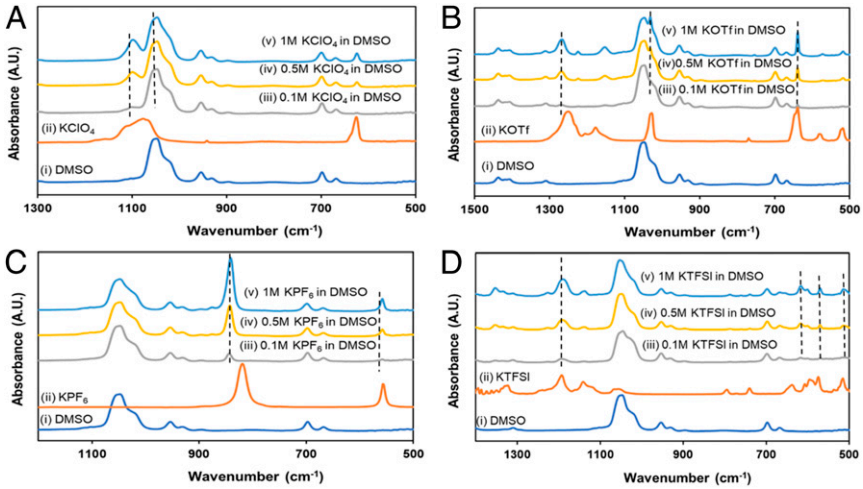

Fig. 3. FTIR spectra of the electrolytes used in this study with various salt concentrations: (*A*) ClO_4^- anion, (*B*) OTf^- anion, (*C*) PF_6^- anion, and (*D*) $TFSI^-$ anion.

The spectra of $KClO_4$/DMSO electrolytes are depicted in Fig. 3*A*. The characteristic spectrum of $KClO_4$ reported elsewhere was readily obtained (62). The broad ClO_4^- peak centered around 1,080 cm^{-1} was observed to split into peaks 1,095 and 1,045 cm^{-1} with the peak at 1,045 cm^{-1} being subsumed by the DMSO ν_{SS} at 1,050 cm^{-1}. At higher salt concentrations, the shoulder to the right of the ν_{SS} peak was found to merge into the overall peak due to the contribution of the salt anion peak. The second prominent ClO_4^- peak centered at 625 cm^{-1} displayed 2 interesting characteristics. First, the peak shifted slightly to 620 cm^{-1} in the electrolyte (1 M) indicating a degree of anion coordination with the K^+ ions, perhaps forming K^+–$(DMSO)_n$–ClO_4^-. However, the relatively small shift coupled with the fact that the peak intensity at 620 cm^{-1} was about a fourth of the intensity measured with the salt itself indicated that the ClO_4^- anions were solvated by DMSO. Thus, the electrolyte consisted of K^+–$(DMSO)_n$–ClO_4^- and $(DMSO)_m$–ClO_4^-.

Fig. 3*B* depicts the spectra for KOTf/DMSO electrolytes. The stretching vibrations of OTF^- appeared at 1,027, 1,175, and 1,246 cm^{-1}, became increasingly prominent with increasing salt concentration, and shifted frequencies with increasing concentration. The stretching vibrations appearing at 1,246 cm^{-1} split into 2 peaks at 1,264 and 1,225 cm^{-1} due to the coordination between the triflate ion and K^+, while the coordination between the S=O of the OTf^- and the K^+ resulted in the observed frequency shifts (61). The comparison of peak intensities at 640 cm^{-1} (chosen so as to not overlap with any DMSO peaks) indicated some degree of anion solvation in this case as well. Thus, the electrolyte contained a combination of predominantly K^+–$(DMSO)_n$–OTf^- with some $(DMSO)_m$–OTf^-.

The spectra of the KPF_6/DMSO electrolytes depicted in Fig. 3*C* offer a significant contrast to the previous 2 cases. The intensities of the characteristic PF_6^- peaks at 555 and 816 cm^{-1} [matching prior reports (61)] in the salt and the electrolyte were found to linearly increase with the salt concentration, and the 816 cm^{-1} peak intensity in the 1 M electrolyte was almost the same as the undissolved salt itself. This indicated minimal (or the absence of) anion solvation. The shifting of the characteristic peaks indicated a degree of coordination of the anion with K^+. The electrolyte consisted mainly of K^+–$(DMSO)_n$–PF_6^- and naked PF_6^-.

The spectra of the KTFSI/DMSO electrolytes are depicted in Fig. 3*D*. Since the $TFSI^-$ anion consists of 2 OTf^- groups attached to a nitrogen, the spectra of the OTf^- and $TFSI^-$ salts share several common features. The asymmetric stretching vibrations at 1,190 cm^{-1} was found to split into 2 peaks at 1,187 and 1,226 cm^{-1} upon coordination of the S=O groups with the K^+ cation. Unlike the OTF^- anion, no significant shift in the peak frequencies is observed in this case. This is a result of the lower charge density of the $TFSI^-$ anion, resulting from the delocalization of the charge across the sulfonyl groups, lowering its Lewis basicity as seen from the lower DN of the $TFSI^-$ compared with OTF^-. The lower Lewis basicity results in poorer coordination with K^+ cations. The peaks corresponding to the salt anion were found to moderately increase in intensity with salt concentration indicating anion solvation. Thus, the electrolyte mainly consists of K^+–$(DMSO)_n$, and $(DMSO)_m$–$TFSI^-$.

Having established that the electrolytes exhibit significant internal variations in solvation structure, the impact on O_2 transport was examined. The diffusion coefficient was calculated using the Nicholson–Shain (N–S) relationship (63, 64) owing to the irreversible nature of the redox process (greater than 60-mV separation between the cathodic and anodic peak potentials as tabulated in *SI Appendix*, Table S3). The N–S plots for electrolytes with different anions are depicted in *SI Appendix*, Fig. S5 *A–D* and were obtained from the cyclic voltammograms (CVs) depicted in *SI Appendix*, Fig. S4 *A–D*. These CVs were recorded at progressively increasing scan rates within the potential window of interest for K–O_2 cells where 1-electron transfer produces KO_2 as the final product [determined for DMSO-based systems in our prior work (5)]. These voltammograms displayed the characteristic 30/α-mV shift in the reduction peak position of the CV for a 10-fold increase in scan rate. The CV characteristics are tabulated in *SI Appendix*, Table S3. The plots were linear with square root of scan rate as expected. The diffusion coefficients calculated from these plots are shown in Fig. 4*A*.

Since the electrophilic O_2 would be solvated by DMSO in all 4 electrolytes and the Stokes–Einstein equation gives an inverse relationship between the radius of the diffusing species and the diffusion coefficient (65), the degree of O_2 solvation may be expected to vary in the order $OTf^- < PF_6^- < TFSI^- < ClO_4^-$. A high DN anion such as OTf^- would display a greater tendency to stay associated with the cation and form K^+–$(solvent)_n$–OTf^- ion pairs compared with PF_6^- with its very low DN. Thus, stabilization of O_2 and O_2^- in an electrolyte is expected to be greater in an electrolyte with a low DN anion (given the same solvent). If the O_2/O_2^- couple is stabilized by ion pair formation, the Stokes radius increases, and the diffusion coefficient would decrease. Furthermore, the activation energy for electron transfer to a stabilized ion pair can be expected to increase, leading to higher overpotentials for both reduction and oxidation. This is reflected in the reversibility of the O_2/O_2^- couple (ΔE_p in *SI Appendix*, Table S3) and the diffusion coefficient in Fig. 4*A* where a correlation is observed.

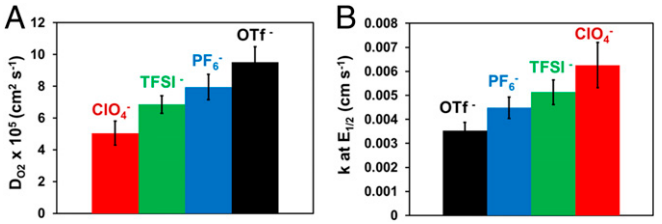

Fig. 4. The impact of the salt anion on the (*A*) diffusion coefficient of O_2 and (*B*) ORR rate constants at the half-wave potential ($E_{1/2}$). The diffusion coefficients were calculated using the N–S equation (CVs in *SI Appendix*, Fig. S4). The ORR rate constants were calculated using the K–L equation (LSVs in *SI Appendix*, Fig. S6). The error bars were calculated from at least 3 independent measurements.

The ORR rate constant was calculated using the Koutecky–Levich (K–L) equation and the relationship $i_K = nFAkC_{O_2}$. The linear sweep voltammograms (LSVs) and their corresponding K–L plots are depicted in *SI Appendix*, Figs. S6 and S7. The calculated rate constants are depicted in Fig. 4*B*. The rate constants were calculated at the half-wave potential (potential at which the current is half the maximum, limiting current of the LSV) to avoid mass transport limitations and provide a comparison independent of variations in O_2 transport.

The combination of a low DN leading to relatively lowered ClO_4^- affinity for the K^+ ion and a high AN leading to facile solvation by DMSO, ensures the predominant formation of $(DMSO)_m$–O_2/K^+–$(DMSO)_n$–O_2^- ion pairs in electrolytes with the ClO_4^- salt. This stabilization of the superoxide promotes the forward reaction and leads to fast first-electron transfer kinetics. The electrolyte with PF_6^- anion has the advantage of a very low DN allowing for the formation of independent K^+–$(DMSO)_n$ species in solution that can go on to associate with O_2/O_2^-. Thus, the first electron transfer kinetics in PF_6^- electrolytes are comparable but lower than that observed ClO_4^- electrolytes. Since the DN of $TFSI^-$ electrolytes is higher than that of PF_6^- by only ~10 kJ·mol^{-1}, very similar behavior to PF_6^- was expected. The FTIR spectra indicated a lack of K^+–$TFSI^-$ coordination, allowing for the formation of independent K^+–$(DMSO)_n$ species in solution that can go on to associate with O_2/O_2^-. The high DN of OTf^- led to the formation of K^+–$(DMSO)_n$–OTf^- ion pairs but also led to poorer O_2/O_2^- stabilization and the slowest first electron transfer rate constants for OTf^- electrolytes. All of the k values measured were in the range of the k_1 values for a Li–O_2 cell (7), confirming that a K–O_2 cell with DMSO-based electrolytes can match the rate capability of a Li–O_2 cell.

The anticorrelation between the diffusion coefficient and the rate constant suggests that the overall performance of a given electrolyte may be described by the Thiele modulus (h_T) (66) with the hydrodynamic radius as the characteristic length. The value of k at $E_{1/2}$ is not mass transport limited and hence satisfies the key boundary condition that the reactant concentration at the surface is finite. This electrochemical Thiele modulus involves a potential dependent k (unlike the constant k in the typical isothermal reaction engineering case). The inherent limitation of the DN and AN of a solvent or the salt to describe the solvation structure in an electrolyte can be overcome by the use of the solvent reorganization energy, which is the amount of energy required to change the solvation shell of the reactants to that of the product during an electrochemical reaction, and which plays a prominent part in the Marcus–Hush kinetic formulation (7, 59, 67). Thus, it encompasses both the ease of solvation of a given species and the ease of oxidizing or reducing it (λ/F may be used to calculate the overpotential required to rearrange or break the solvation shell of a given reactant).

Plots of $\ln(h_T)^2$ vs. λ are depicted in Fig. 5. To establish the possible universality of this correlation, ORR rate constants and O_2 diffusion coefficients for Li–O_2 and Na–O_2 cells from the literature (61, 68, 69) were used in Fig. 5. The calculation of λ is detailed in *SI Appendix*, section S7. For all 3 systems, the following relationship was observed:

$$(h_T)^2 = \frac{kr_{hyd}}{D_{O_2}} = Ae^{B\lambda}. \quad [1]$$

The parameters A and B are tabulated in *SI Appendix*, Table S4. The difference between the highest and lowest λ values increased with cation size, while A increased by an order of magnitude from Li to Na to K. As the ionic radius increases (and charge density decreases), the hardness of the cation is lowered and enables easier formation of M^+–$(solvent)_n$–O_2^- complexes while also increasing the competition between O_2^- and the anions (which are typically soft bases). Thus, selection of the salt anion becomes increasingly important when moving to larger cations, while the solvent itself is important in case of Li^+ (43, 70). The physical origin of this empirical relationship was identified by modeling the system as detailed in *SI Appendix*, Fig. S11. The model is built for glassy carbon electrode with an O_2 concentration gradient across the boundary layer. This 1D model derives an expression for the electrochemical Thiele modulus incorporating the solvent reorganization energy (λ) concept from Marcus–Hush theory. The final expression for the electrochemical Thiele modulus is as follows:

$$h_T^2 = \left(\frac{kL^2}{D_{O_2}}\right) = \left(\frac{i_o e^{\left(-\frac{4RT\eta\lambda}{F}\right)} L^2}{nF(C_{O_2})_{bulk} D_{O_2}}\right). \quad [2]$$

Thus, the empirical parameters A and B are given by the following:

$$A = \frac{i_0 L^2}{nF(C_{O_2})_{bulk} D_{O_2}}, \quad [3]$$

$$B = -\frac{4RT\eta}{F}. \quad [4]$$

Herein, A captures the transport dependencies, while B captures the overpotential driving force.

The practical impact of the counterion selection on battery performance was determined using symmetric cells to obtain polarization measurements with the electrolytes of interest. The experimental setup of the symmetric cells used is described in *SI*

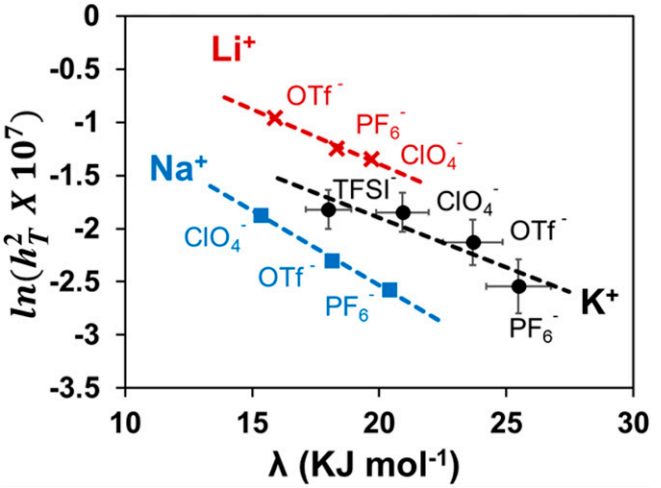

Fig. 5. Correlation between the solvent reorganization energy (λ), the O_2 diffusion coefficient (D_{O_2}), and the first electron transfer rate constant (k).

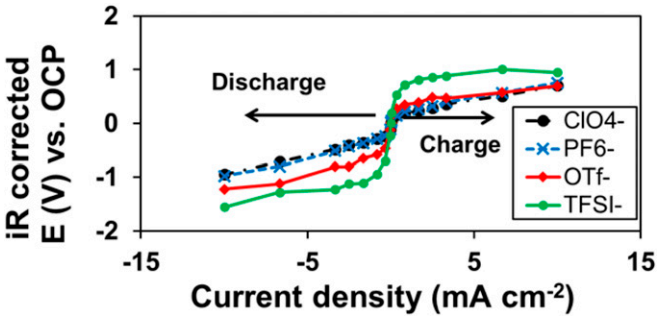

Fig. 6. Charge–discharge polarization curves for symmetric cells using O_2-saturated DMSO-based K^+ electrolytes with various anions.

Appendix. The choice of using a symmetric cell as opposed to a full K–O_2 cell was deliberate. The use of DMSO-based electrolytes precludes the use of metallic K anodes due to the carbon–sulfur bond cleavage reaction (29), and would require the use of intercalation or alloy anodes that may potentially mitigate this issue. Practical DMSO-based K–O_2 cells have been reported (40, 71) but introduce several other cell components (such as a poorly conductive ceramic separator), which would make isolating and examining the impact of just the electrolyte challenging. Thus, to conclusively demonstrate that any performance difference is only due to the choice of the electrolyte, we used symmetric cells where the only variable was the electrolyte. The setup of these cell is described in greater detail in Sankarasubramanian and Ramani (5). The cells were continuously purged with oxygen to ensure the same oxygen content in the electrolyte at all times. The cells were charged and discharged at constant current to a capacity of 0.1 mAh at a series of current densities. Three cycles were carried out at each current density followed by a 20-min period where the open-circuit potential was monitored followed by the subsequent cycles. The iR corrected charge and discharge polarization curves are presented in Fig. 6. Current densities higher than 10 mA/cm^2 were not examined to avoid entering O_2 starvation conditions.

The formation of KO_2 as the discharge product on the electrodes was confirmed by EDAX and Raman spectroscopy (*SI Appendix*, Figs. S11 and S12). The choice of electrolyte anion was found to have no impact on the decomposition of the KO_2 product during the charge process except in the case of the KTFSI electrolyte. This is consistent with the fact that KO_2 formed in the solution or the surface can be expected to partially deposit or precipitate onto the electrode. The KTFSI electrolyte may lead preferential deposition of the KO_2 on the surface and the higher charge overpotential may be a consequence of the increased resistance. This hypothesis is supported by higher measured overall cell resistances after cycling of the KTFSI-based cell. Thus, the electrolyte properties are largely immaterial to the charging process except at current densities higher than those examined here where limitations due to ion transport rates may be observed. The trends observed for the discharge process followed the kinetic trends from the rotating disk electrode (RDE) measurements. Both ClO_4^- and PF_6^- electrolytes showed similar discharge polarization performance, but the higher diffusion coefficient value and the facile solvation behavior in PF_6^- electrolytes lead us to recommend DMSO electrolytes incorporating this anion as the best option for high-current K–O_2 cells.

From a practical standpoint, the critical performance metric for any proposed high-power battery system are the discharge rate and overpotential. The 200- to 300-mV lower overpotential achievable at 10 mA·cm^{-2} current density using our approach will lead to significant improvements in energy efficiency of the battery and allow the attainment of even higher discharge rates.

Materials and Methods

The chemicals list, supplier details, preparation procedures, and characterization methods are detailed in *SI Appendix*. The electrochemical measurements were carried out using a 3-electrode configuration water jacketed, 5-neck electrochemical cell with suitable openings for the working, counter, and reference electrodes, the gas purge line inlet, and a gas outlet (Pine Instruments; AKCELL3) (5). A glassy carbon RDE was used as the working electrode. The counter electrode consisted of a Pt spiral attached to a Pt wire in a fritted glass tube filled with the electrolyte. The reference electrode consisted of an Ag wire immersed in an CH_3CN solution of 10 mM $AgNO_3$ and 0.1 M $TBACF_3SO_3$ in a fritted glass tube. All potentials reported in this study are vs. $Ag/AgNO_3$, unless otherwise noted. The reference electrode was calibrated to the ferrocene/ferrocenium scale following the International Union of Pure and Applied Chemistry recommendations outlined in Gritzner and Kuta (5, 72). The reference electrode calibration can be found in *SI Appendix*.

The K–O_2 symmetric cell [detailed previously in Sankarasubramanian and Ramani (5)] consisted of a sealed 3-neck, round-bottom flask with activated carbon felt working and counter electrodes and a glass fritted gas sparge for O_2 bubbling. The polarization measurements were carried out in a 2-electrode configuration with independent leads for the current and potential. The potentials were measured against the $K^+_{(in\ solution)} + e^- \leftrightarrow K_{(deposition)}$ reaction at the anode (counter electrode).

Conclusions

The ORR rate in the presence of alkali metal ions was found to increasingly depend on the choice of salt anion as the cation size increased. The O_2 diffusion coefficients in the electrolyte were found to be a complex function of the solvent and salt anion DN and AN. The reversibility of the ORR and the O_2 diffusion coefficient ($ClO_4^- < TFSI^- < PF_6^- < OTf^-$) were directly correlated. The trend for the first electron transfer rate constants was the exact reverse ($OTf^- < PF_6^- < TFSI^- < ClO_4^-$) and was found to translate unchanged from the RDE to the symmetric cell. Overall, it was demonstrated that the solvent reorganization energy correlates well with the Thiele modulus (which in turn captures the ORR kinetics and O_2 diffusion coefficient in the electrolytes) and overall cell-scale performance requires electrolytes exhibiting either high or low λ over the course of the ORR. Notably, an expression for the electrochemical Thiele modulus incorporating elements of Marcus–Hush kinetics has been developed. Electrolytes with poorly solvated anions, and high λ were found to exhibit the lowest discharge polarization and hence highest discharge rate capability in practical systems, allowing for the realization of relatively high-power output from alkali metal–air batteries. In summary, effective solvation will greatly influence the discharge rate of alkali metal–oxygen batteries with the choice of both solvent and salt becoming increasingly crucial with larger alkali metal cations. The combination of comparatively higher diffusion coefficients, facile solvation, and 200-mV lower discharge overpotential in KPF_6/DMSO renders it the best electrolyte for high-power K–O_2 cells.

ACKNOWLEDGMENTS. We gratefully acknowledge Washington University in St. Louis McKelvey School of Engineering and the Roma B. and Raymond H. Wittcoff Distinguished University Professorship for enabling this study. The microscopy and FTIR spectroscopy reported in this work were performed at the Nano Research Facility, which is supported by the National Science Foundation under Grant ECS-0335765.

1. J. Christensen *et al.*, A critical review of Li/air batteries. *J. Electrochem. Soc.* **159**, R1–R30 (2012).
2. K. M. Abraham, Prospects and limits of energy storage in batteries. *J. Phys. Chem. Lett.* **6**, 830–844 (2015).
3. Department of Energy, Funding opportunity announcement: Advanced Research Projects Agency–Energy (Arpa-E) duration addition to electricity storage (DAYS) (DE-FOA-0001906, Department of Energy, 2017). https://arpa-e.energy.gov/?q=pdfs/days-de-foa-0001906. Accessed 1 May 2018.
4. K. M. Abraham, Z. Jiang, A polymer electrolyte-based rechargeable lithium/oxygen battery. *J. Electrochem. Soc.* **143**, 1–5 (1996).
5. S. Sankarasubramanian, V. Ramani, Dimethyl sulfoxide-based electrolytes for high-current potassium-oxygen batteries. *J. Phys. Chem. C* **122**, 19319–19327 (2018).
6. S. Sankarasubramanian, J. Seo, F. Mizuno, N. Singh, J. Prakash, Rotating ring-disc electrode investigation of the aprotic superoxide radical electrochemistry on multi-crystalline surfaces and correlation with density functional theory modeling: Implications for lithium-air cells. *J. Electrochem. Soc.* **163**, A2377–A2384 (2016).

7. S. Sankarasubramanian, J. Seo, F. Mizuno, N. Singh, J. Prakash, Elucidating the oxygen reduction reaction kinetics and the origins of the anomalous tafel behavior at the lithium-oxygen cell cathode. *J. Phys. Chem. C* **121**, 4789–4798 (2017).
8. A. Débart, A. J. Paterson, J. Bao, P. G. Bruce, α-MnO_2 nanowires: a catalyst for the O_2 electrode in rechargeable lithium batteries. *Angew. Chem.* **47**, 4521–4524 (2008).
9. P. G. Bruce, S. A. Freunberger, L. J. Hardwick, J. M. Tarascon, Li-O_2 and Li-S batteries with high energy storage. *Nat. Mater.* **11**, 19–29 (2011). Erratum in: *Nat. Mater.* **11**, 172 (2012).
10. H.-G. Jung, J. Hassoun, J.-B. Park, Y.-K. Sun, B. Scrosati, An improved high-performance lithium-air battery. *Nat. Chem.* **4**, 579–585 (2012).
11. R. S. Assary, K. C. Lau, K. Amine, Y.-K. Sun, L. A. Curtiss, Interactions of dimethoxy ethane with Li_2O_2 clusters and likely decomposition mechanisms for Li–O_2 batteries. *J. Phys. Chem. C* **117**, 8041–8049 (2013).
12. S. A. Freunberger *et al*., Reactions in the rechargeable lithium-O_2 battery with alkyl carbonate electrolytes. *J. Am. Chem. Soc.* **133**, 8040–8047 (2011).
13. S. A. Freunberger *et al*., The lithium-oxygen battery with ether-based electrolytes. *Angew. Chem. Int. Ed. Engl.* **50**, 8609–8613 (2011).
14. F. Mizuno *et al*., Cathode reaction mechanism of non-aqueous Li-O_2 batteries with highly oxygen radical stable electrolyte solvent. *J. Power Sources* **228**, 47–56 (2013).
15. Y.-C. Lu, H. A. Gasteiger, M. C. Parent, V. Chiloyan, Y. Shao-Horn, The influence of catalysts on discharge and charge voltages of rechargeable Li–oxygen batteries. *Electrochem. Solid State Lett.* **13**, A69 (2010).
16. Y. C. Lu, H. A. Gasteiger, Y. Shao-Horn, Catalytic activity trends of oxygen reduction reaction for nonaqueous Li-air batteries. *J. Am. Chem. Soc.* **133**, 19048–19051 (2011).
17. Y. C. Lu *et al*., Platinum-gold nanoparticles: A highly active bifunctional electro-catalyst for rechargeable lithium-air batteries. *J. Am. Chem. Soc.* **132**, 12170–12171 (2010).
18. S. Sankarasubramanian, N. Singh, F. Mizuno, J. Prakash, Ab initio investigation of the oxygen reduction reaction activity on noble metal (Pt, Au, Pd), Pt 3 M (M = Fe, Co, Ni, Cu) and Pd 3 M (M = Fe, Co, Ni, Cu) alloy surfaces, for Li O_2 cells. *J. Power Sources* **319**, 202–209 (2016).
19. S. H. Oh, R. Black, E. Pomerantseva, J. H. Lee, L. F. Nazar, Synthesis of a metallic mesoporous pyrochlore as a catalyst for lithium–O2 batteries. *Nat. Chem.* **4**, 1004–1010 (2012).
20. S. H. Oh, L. F. Nazar, Oxide catalysts for rechargeable high-capacity Li-O_2 batteries. *Adv. Energy Mater.* **2**, 903–910 (2012).
21. F. Mizuno, T. S. Arthur, K. Takechi, Water in ionic liquid for electrochemical Li cycling. *ACS Energy Lett.* **1**, 542–547 (2016).
22. S. Sankarasubramanian *et al*., Enhancement of oxygen reduction reaction rate by addition of water to an oxidatively stable ionic liquid electrolyte for lithium-air cells. *Electrochem. Commun.* **73**, 55–58 (2016).
23. J. Lu *et al*., A lithium-oxygen battery based on lithium superoxide. *Nature* **529**, 377–382 (2016).
24. K. G. Gallagher *et al*., Quantifying the promise of lithium-air batteries for electric vehicles. *Energy Environ. Sci.* **7**, 1555–1563 (2014).
25. P. Adelhelm *et al*., From lithium to sodium: Cell chemistry of room temperature sodium-air and sodium-sulfur batteries. *Beilstein J. Nanotechnol.* **6**, 1016–1055 (2015).
26. P. Hartmann *et al*., A rechargeable room-temperature sodium superoxide (NaO_2) battery. *Nat. Mater.* **12**, 228–232 (2013).
27. P. Hartmann *et al*., A comprehensive study on the cell chemistry of the sodium superoxide (NaO_2) battery. *Phys. Chem. Chem. Phys.* **15**, 11661–11672 (2013).
28. C. Xia, R. Black, R. Fernandes, B. Adams, L. F. Nazar, The critical role of phase-transfer catalysis in aprotic sodium oxygen batteries. *Nat. Chem.* **7**, 496–501 (2015).
29. D. E. O'Connor, W. I. Lyness, The reaction of sodium and potassium with dimethyl sulfoxide. The formation and alkylation of methanesulfenate1. *J. Org. Chem.* **30**, 1620–1623 (1965).
30. T. Shiga, Y. Hase, Y. Kato, M. Inoue, K. Takechi, A rechargeable non-aqueous Mg-O_2 battery. *Chem. Commun. (Camb.)* **49**, 9152–9154 (2013).
31. D. Aurbach *et al*., A short review on the comparison between Li battery systems and rechargeable magnesium battery technology. *J. Power Sources* **97–98**, 28–32 (2001).
32. R. Mohtadi, F. Mizuno, Magnesium batteries: Current state of the art, issues and future perspectives. *Beilstein J. Nanotechnol.* **5**, 1291–1311 (2014).
33. P. Reinsberg, C. J. Bondue, H. Baltruschat, Calcium–oxygen batteries as a promising alternative to sodium–oxygen batteries. *J. Phys. Chem. C* **120**, 22179–22185 (2016).
34. X. Ren, Y. Wu, A low-overpotential potassium-oxygen battery based on potassium superoxide. *J. Am. Chem. Soc.* **135**, 2923–2926 (2013).
35. N. Xiao, X. Ren, M. He, W. D. McCulloch, Y. Wu, Probing mechanisms for inverse correlation between rate performance and capacity in K-O_2 batteries. *ACS Appl. Mater. Interfaces* **9**, 4301–4308 (2017).
36. W. D. McCulloch, X. Ren, M. Yu, Z. Huang, Y. Wu, Potassium-ion oxygen battery based on a high capacity antimony anode. *ACS Appl. Mater. Interfaces* **7**, 26158–26166 (2015).
37. X. Ren *et al*., Understanding side reactions in K-O_2 batteries for improved cycle life. *ACS Appl. Mater. Interfaces* **6**, 19299–19307 (2014).
38. N. Xiao, G. Gourdin, Y. Wu, Simultaneous stabilization of potassium metal and superoxide in K-O_2 batteries on the basis of electrolyte reactivity. *Angew. Chem. Int. Ed. Engl.* **57**, 10864–10867 (2018).
39. N. Xiao, R. T. Rooney, A. A. Gewirth, Y. Wu, The long-term stability of KO_2 in K-O_2 batteries. *Angew. Chem. Int. Ed. Engl.* **57**, 1227–1231 (2018).
40. W. Wang, N. C. Lai, Z. Liang, Y. Wang, Y. C. Lu, Superoxide stabilization and a universal KO_2 growth mechanism in potassium-oxygen batteries. *Angew. Chem. Int. Ed. Engl.* **57**, 5042–5046 (2018).
41. N. Xiao, X. Ren, W. D. McCulloch, G. Gourdin, Y. Wu, Potassium superoxide: A unique alternative for metal–air batteries. *Acc. Chem. Res.* **51**, 2335–2343 (2018).
42. C. O. Laoire, S. Mukerjee, K. M. Abraham, E. J. Plichta, M. A. Hendrickson, Influence of nonaqueous solvents on the electrochemistry of oxygen in the rechargeable lithium-air battery. *J. Phys. Chem. C* **114**, 9178–9186 (2010).
43. C. J. Allen *et al*., Oxygen reduction reactions in ionic liquids and the formulation of a general ORR mechanism for Li-air batteries. *J. Phys. Chem. C* **116**, 20755–20764 (2012).
44. M. J. Trahan, S. Mukerjee, E. J. Plichta, M. A. Hendrickson, K. M. Abraham, Studies of Li-air cells utilizing dimethyl sulfoxide-based electrolyte. *J. Electrochem. Soc.* **160**, A259–A267 (2013).
45. L. Lutz *et al*., Role of electrolyte anions in the Na-O_2 battery: Implications for NaO_2 solvation and the stability of the sodium solid electrolyte interphase in glyme ethers. *Chem. Mater.* **29**, 6066–6075 (2017).
46. D. Sawyer, G. C. Jr, Effects of media and electrode materials on the electrochemical reduction of dioxygen. *Anal. Chem.* **2**, 1720–1724 (1982).
47. H. M. A. Amin, C. Molls, P. P. Bawol, H. Baltruschat, The impact of solvent properties on the performance of oxygen reduction and evolution in mixed tetraglyme-dimethyl sulfoxide electrolytes for Li-O_2 batteries: Mechanism and stability. *Electrochim. Acta* **245**, 967–980 (2017).
48. I. Gunasekara, S. Mukerjee, E. J. Plichta, M. A. Hendrickson, K. M. Abraham, A study of the influence of lithium salt anions on oxygen reduction reactions in Li-air batteries. *J. Electrochem. Soc.* **162**, A1055–A1066 (2015).
49. W. Walker *et al*., A rechargeable Li-O_2 battery using a lithium nitrate/*N*,*N*-dimethylacetamide electrolyte. *J. Am. Chem. Soc.* **135**, 2076–2079 (2013).
50. N. B. Aetukuri *et al*., Solvating additives drive solution-mediated electrochemistry and enhance toroid growth in non-aqueous Li-O_2 batteries. *Nat. Chem.* **7**, 50–56 (2015).
51. C. M. Burke, V. Pande, A. Khetan, V. Viswanathan, B. D. McCloskey, Enhancing electrochemical intermediate solvation through electrolyte anion selection to increase nonaqueous Li-O_2 battery capacity. *Proc. Natl. Acad. Sci. U.S.A.* **112**, 9293–9298 (2015).
52. I. Landa-Medrano *et al*., Potassium salts as electrolyte additives in lithium-oxygen batteries. *J. Phys. Chem. C* **121**, 3822–3829 (2017).
53. K. U. Schwenke, M. Metzger, T. Restle, M. Piana, H. A. Gasteiger, The influence of water and protons on Li_2O_2 crystal growth in aprotic Li-O_2 cells. *J. Electrochem. Soc.* **162**, A573–A584 (2015).
54. V. Gutmann, Solvent effects on the reactivities of organometallic compounds. *Coord. Chem. Rev.* **18**, 225–255 (1976).
55. V. Gutmann, Empirical parameters for donor and acceptor properties of solvents. *Electrochim. Acta* **21**, 661–670 (1976).
56. M. Holzweber *et al*., Mutual Lewis acid-base interactions of cations and anions in ionic liquids. *Chemistry* **19**, 288–293 (2013).
57. D. J. Eyckens, L. C. Henderson, A review of solvate ionic liquids: Physical parameters and synthetic applications. *Front Chem.* **7**, 263 (2019).
58. M. Schmeisser, P. Illner, R. Puchta, A. Zahl, R. van Eldik, Gutmann donor and acceptor numbers for ionic liquids. *Chemistry* **18**, 10969–10982 (2012).
59. P. Bai, M. Z. Bazant, Charge transfer kinetics at the solid-solid interface in porous electrodes. *Nat. Commun.* **5**, 3585 (2014).
60. J. Coates, "Interpretation of infrared spectra, a practical approach" in *Encyclopedia of Analytical Chemistry*, R. A. Meyers, Ed. (Wiley, 2006), pp. 1–23.
61. I. Gunasekara, S. Mukerjee, E. J. Plichta, M. A. Hendrickson, K. M. Abraham, Micro-electrode diagnostics of lithium-air batteries. *J. Electrochem. Soc.* **161**, A381–A392 (2014).
62. F. A. Miller, C. H. Wilkins, Infrared spectra and characteristic frequencies of inorganic ions. *Anal. Chem.* **20**, 1253–1294 (1952).
63. R. S. Nicholson, Theory and application of cyclic voltammetry for measurement of electrode reaction kinetics. *Anal. Chem.* **37**, 1351–1355 (1965).
64. R. S. Nicholson, I. Shain, Theory of stationary electrode polarography: Single scan and cyclic methods applied to reversible, irreversible, and kinetic systems. *Anal. Chem.* **36**, 706–723 (1964).
65. C. C. Miller, The Stokes-Einstein law for diffusion in solution. *Proc. R. Soc. A Math. Phys. Eng. Sci.* **106**, 724–749 (1924).
66. E. W. Thiele, Relation between catalytic activity and size of particle. *Ind. Eng. Chem.* **31**, 916–920 (1939).
67. E. Laborda, M. C. Henstridge, C. Batchelor-McAuley, R. G. Compton, Asymmetric Marcus-Hush theory for voltammetry. *Chem. Soc. Rev.* **42**, 4894–4905 (2013).
68. V. S. Dilimon *et al*., Superoxide stability for reversible Na-O_2 electrochemistry. *Sci. Rep.* **7**, 17635 (2017).
69. C. J. Bondue, P. Reinsberg, A. A. Abd-El-Latif, H. Baltruschat, Oxygen reduction and oxygen evolution in DMSO based electrolytes: The role of the electrocatalyst. *Phys. Chem. Chem. Phys.* **17**, 25593–25606 (2015).
70. C. O. Laoire, S. Mukerjee, K. M. Abraham, E. J. Plichta, M. A. Hendrickson, Elucidating the mechanism of oxygen reduction for lithium-air battery applications. *J. Phys. Chem. C* **113**, 20127–20134 (2009).
71. G. Cong, W. Wang, N.-C. Lai, Z. Liang, Y.-C. Lu, A high-rate and long-life organic-oxygen battery. *Nat. Mater.* **18**, 390–396 (2019).
72. G. Gritzner, J. Kuta, Recommendations on reporting electrode potentials in non-aqueous solvents (Recommendations 1983). *Pure Appl. Chem.* **56**, 461–466 (1984).